Engineering Metal–Organic Frameworks for the Electrochemical Reduction of CO$_2$

A Minireview

Wang, Riming; Kapteijn, Freek; Gascon, Jorge

Important note
To cite this publication, please use the final published version (if applicable).
Please check the document version above.

Special Issue
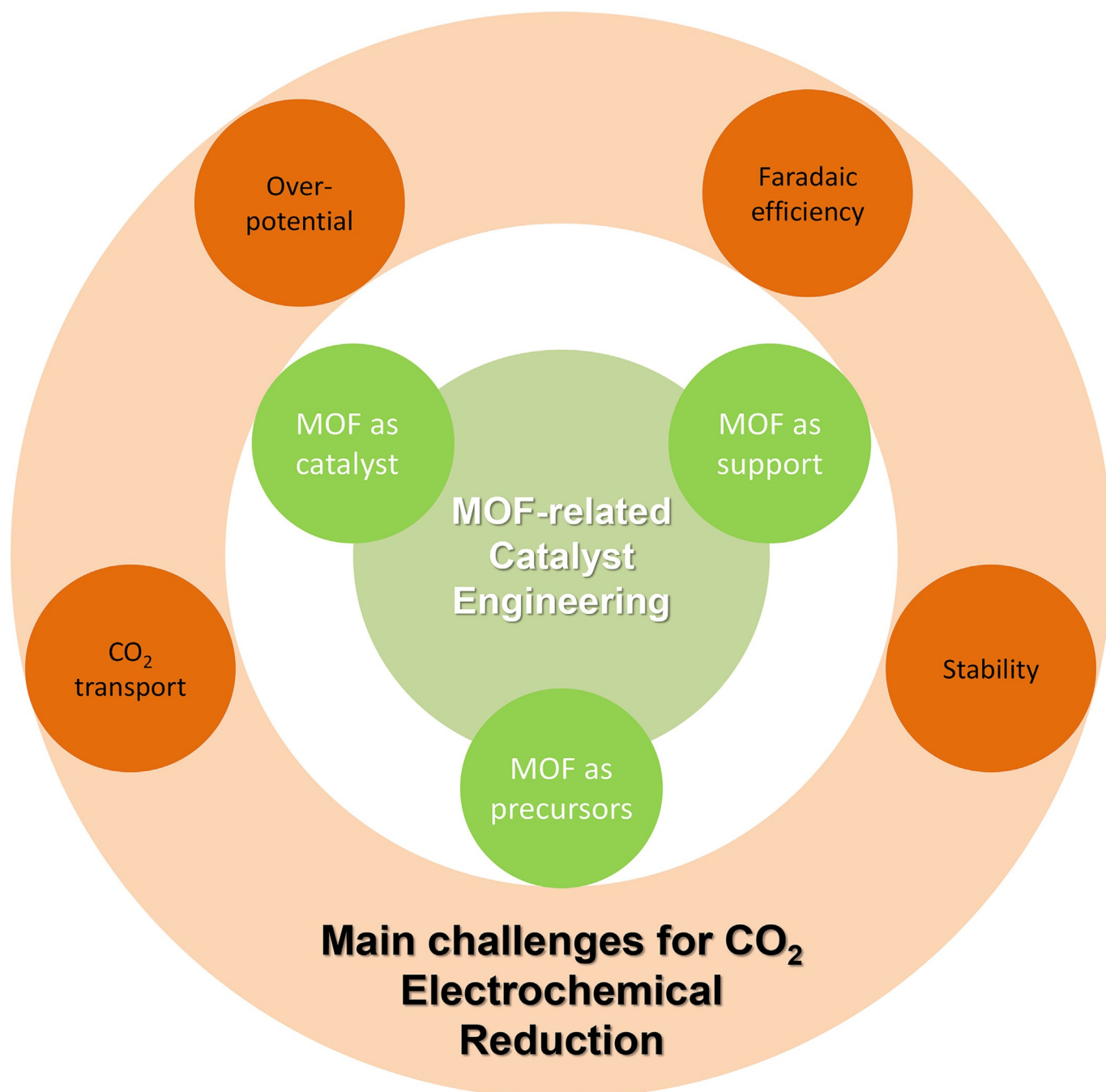
Engineering Metal–Organic Frameworks for the Electrochemical Reduction of CO$_2$: A Minireview

Riming Wang,[a] Freek Kapteijn,[a] and Jorge Gascon*[a, b]

Over-potential

Faradaic efficiency

MOF as catalyst

MOF as support

MOF-related Catalyst Engineering

CO$_2$ transport

Stability

MOF as precursors

Main challenges for CO$_2$ Electrochemical Reduction

Abstract: The electrochemical reduction of CO_2 holds great promise for lowering the concentration of CO_2 in the Earth's atmosphere. However, several challenges have hindered the commercialization of this technology, including energy efficiency, the solubility of CO_2 in the aqueous phase, and electrode stability. In this Minireview, we highlight and summarize the main advantages and limitations that metal–organic frameworks (MOFs) may offer in this field of research, either when used directly as electrocatalysts or when used as catalyst precursors.

1. Introduction

The ever-increasing concentration of CO_2 in the Earth's atmosphere is one of the most urgent and critical issues facing humanity. From the point of view of the global carbon cycle, industrial activity is the major contributor to CO_2 emission, thereby causing the rapid accumulation of this greenhouse gas in the atmosphere. To counteract this imbalance, the implementation of CO_2-capture and -utilization technologies is required. In this spirit, several technologies have been proposed for CO_2 utilization, which are typically based on thermocatalysis, photocatalysis, and electrocatalysis. All of these approaches have their own economic advantages under certain conditions, and they may all contribute to cutting the concentration of atmospheric CO_2.[1] For example, thermocatalysis would already be economically competitive if "green" hydrogen (e.g., generated from water splitting by using renewable energy) were readily available on a mass scale.[2] On the other hand, photocatalysis is more favorable in remote locations with strong solar irradiation. The electrocatalytic reduction of CO_2 (CO_2ER) is the other technology that holds great promise if efficient electrocatalysts can be developed for the direct transformation of CO_2 into valuable products.

Initial CO_2ER catalysts were pure-metal foils that were directly used as electrodes.[3] However, since the advancement of nanotechnology, other configurations have been employed as catalysts for the CO_2ER with significantly enhanced efficiency.[4] In these nanostructured electrocatalysts, the active phase is dispersed within a conductive support, such as carbon cloth, carbon paper, or glassy carbon. In the following context, "electrode" mainly refers to catalysts that are dispersed on a conductive support, and "catalyst engineering" represents the engineering effort to improve CO_2ER efficiency (including Faradaic efficiencies toward valuable products, current densities, and energy efficiencies) through the design of catalytic sites and/or optimization of the catalyst structure.

Recently, metal–organic frameworks (MOFs) have gained increasing interest in the field of catalysis because of their unique textural and topological properties.[5] On the one hand, when MOFs are used directly as catalysts, not only can the atomically dispersed metal nodes be engineered into active sites, but also the organic linkers hold great potential as catalytic sites.[6] Furthermore, their porous structure can be tuned to enhance mass transport. On the other hand, MOFs can also be used as catalyst precursors, thereby affording MOF-mediated catalysts.[7] In this approach, a MOF is decomposed under controlled conditions to induce clustering of its metal component into small nanoparticles or the formation of single-atom catalytic sites. At the same time, an organic component (the linker) rearranges into a carbonaceous matrix that may be conductive.[8] Xia et al. reviewed the use of MOFs in electrochemical energy storage, including catalytic electrodes.[9] Herein, we summarize the recent advances in the electrochemical reduction CO_2 by using MOF and MOF-derived catalysts.

To review the work done so far on this interesting topic, we must realize that the commercialization of the CO_2ER does not solely rely on catalyst engineering. Indeed, the design of the electrochemical cell and optimization of the reaction conditions (pressure, temperature, etc.) will also play a role as important as that of the catalyst itself.

In this Minireview, we begin by briefly introducing the challenges facing CO_2ER, followed by a summary of MOF-related catalyst engineering and MOF-derived electrocatalysts. We will conclude with our personal opinion on the future developments in this area.

2. Main Challenges Facing CO₂ER

The electrochemical reduction of CO_2 (CO_2ER) can be considered as the reverse process to that used in fuel cells, and a lot of similarities are shared between these two processes, such as cell configuration and an electrolyte. CO_2ER with a hydrogen cell, which is among the most popular cell configurations developed to date, features cathode and anode compartments that are filled with an aqueous electrolyte and separated by a membrane. MOF and MOF-derived catalysts are mostly particles, and are used as supported catalysts in CO_2ER cells. The CO_2 molecules approach the catalytic sites through diffusion in the aqueous phase, and several valuable products can be generated, such as CO, C_2H_4, HCOOH, oxalic acid, and alcohols. As

[a] R. Wang, Prof. Dr. F. Kapteijn, Prof. Dr. J. Gascon
Catalysis Engineering
Chemical Engineering Department
Delft University of Technology
Van der Maasweg 9
2629 HZ Delft (Netherlands)
E-mail: jorge.gascon@kaust.edu.sa

[b] Prof. Dr. J. Gascon
Advanced Catalytic Materials
KAUST Catalysis Center
King Abdullah University of Science and Technology
Thuwal 23955 (Saudi Arabia)

(iD) The ORCID identification number(s) for the author(s) of this article can be found under:
https://doi.org/10.1002/asia.201900710.

proposed by Koper and co-workers,[10] the reduction of CO_2 begins with the formation of a $\cdot COO^-$ intermediate. Subsequent reaction with a proton–electron pair leads to the formation of $HCOO^-$, whilst the absorption of only a proton results in the formation of $\cdot COOH$, which is further reduced into $\cdot CO$. On the one hand, if the $\cdot CO$ intermediate is strongly bound by the metal (e.g. Cu), it will be reduced into additional products; on the other hand, if the $\cdot CO$ intermediate is weakly bound by the metal (e.g., Ag, Au, or Zn), CO will desorb and become the main product.

The challenges facing CO_2ER have been widely summarized and discussed elsewhere,[1, 11] so we will only give a brief introduction to CO_2ER herein, with specific emphasis on commercialization considerations.

2.1. Overpotential (Voltage Efficiency)

One of the key drawbacks that hinder the commercialization of the CO_2ER is its energy efficiency, which is primarily limited by the high overpotential of the CO_2ER.

In electrochemistry, overpotential is the potential (voltage) difference between the reduction potential of a half reaction at thermodynamic equilibrium and the potential at which the redox reaction occurs. The existence of an overpotential implies that more energy is required than is thermodynamically needed to drive a given reaction, and this energy loss, usually as thermal energy, directly affects voltage efficiency.

It is widely accepted that the overpotential for the electrochemical reduction of CO_2 originates from the sluggish kinetics to form a $\cdot CO_2^-$ intermediate.[11a, c] This step has a standard potential of -1.9 V (vs. standard hydrogen electrode, SHE) and is the main reason for the high overpotentials. This potential can be improved (lowered) by stabilizing the intermediate, which is one of the primary functions of the catalysts.

2.2. Faradaic Efficiency (FE)

Faraday efficiency is described as energy losses in the current term. Although all of the current in the CO_2ER is consumed to form products, the current that is directed towards undesirable reactions or products is usually considered as energy loss.

One primary undesirable product is H_2, which is generated by the competing hydrogen-evolution reaction (HER) in the aqueous electrolyte. As a consequence, catalysts with high hydrogen overpotentials typically give favorable FEs for CO_2ER.

From a commercialization perspective, the potential market for CO_2ER is primarily fuel and commodity chemicals, in which oil-derived products are currently predominant. Taking the competition between CO_2ER derived chemicals and petrochemicals into consideration, it is clear that some CO_2ER products, such as CH_4, are economically unfavorable. Therefore, the formation of these products should be avoided, because the electricity cost to produce them will not be paid off.[1]

One scenario for the commercialization of CO_2ER would be the direct treatment of post-combustion gas from power plants, which would avoid the need for expensive (and highly energy consuming) separation. These streams typically contain a relatively high concentration of unreacted O_2. Thus, CO_2ER catalysts for this specific application should be inactive for the oxygen-reduction reaction (ORR).[12] Moreover, the products of the ORR can include reactive O_2^- and H_2O_2 species, which would provide a harmful environment for CO_2ER catalysts.[13]

2.3. CO_2 Mass Transport

One of the key limiting factors in the aqueous-phase conversion of CO_2 is its mass transfer to the cathode surface, in particular given the low solubility of CO_2 in many electrolytes. In

Riming Wang received his M.Sc. degree in 2015 from the College of Material Science and Engineering, Shandong University. Then, he joined the Department of Chemical Engineering at Delft University of Technology as a PhD student, under the supervision of Prof. Freek Kapteijn and Prof. Jorge Gascon. His research focuses on MOF-mediated catalyst engineering for the electrochemical reduction of CO_2 and MOF-promoted photocatalysis.

Freek Kapteijn (1952), MSc in Chemistry and Mathematics, received his Ph.D. in 1980 from the University of Amsterdam. After holding Postdoctoral positions in Amsterdam (Coal Science) and Nancy (ENSIC), he took up a position as Associate Professor at the University of Amsterdam. He later moved to Delft University of Technology in 1992, where he was appointed "Anthonie van Leeuwenhoek Professor" in 1999, and held the post of Chair of the Catalysis Engineering team from 2008–2019. He has received the prestigious Golden Hoogewerff award and was among the most highly cited scientists in the "cross-field" category in 2018 by Clarivate Analytics. His research interests focus on the interplay between catalysis and engineering, which comprises structured and multifunctional catalysts, adsorption, separation, and (catalytic) membranes. He has co-authored over 650 publications in peer-reviewed journals and book chapters.
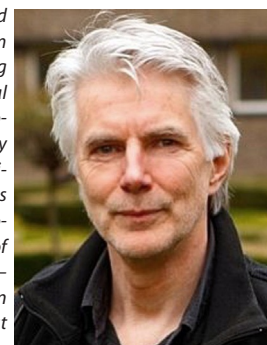
Jorge Gascon (1977) was born in Huesca (Spain) and received his M.Sc. in Chemistry (2002) and his Ph.D. in Chemical Engineering (2006) from the University of Zaragoza (Spain). He held the positions of Postdoctoral Research Officer (2006–2009), Assistant Professor (2010–2012), Associate Professor (2012–2014), and Antoni van Leeuwenhoek Professor (2014–2017) of Catalysis Engineering at TU-Delft (NL). Since 2017, he has held the position Professor of Chemical and Biological Engineering and Director at the KAUST Catalysis Center. He is a member of the board of the International Zeolite Association Commission on Metal–Organic Frameworks. He was the recipient of the 2013 ExxonMobil Chemical European Science and Engineering Award and he is a 2018 Clarivate Analytics highly cited researcher. His research focuses on the development of sustainable technologies for the production of chemicals, energy carriers, and new environmental applications.

addition to the CO_2 capacity of the catholyte, the formation of product bubbles can also disrupt the reaction system. Although the low solubility of CO_2 in the aqueous phase can be overcome by using gas-diffusion electrodes (GDEs), the current density of cathode GDEs may also be limited by CO_2 flux to the catalyst. The CO_2-transport limit is considered to be the critical issue that hinders the enhancement of current density.[14] The configuration of electrochemical cells may largely influence CO_2 transportation and, in turn, the current density; thus, a comparison of current densities should also take the cell configuration into account.[15]

2.4. Electrode Stability

Stability is an essential criterion for commercial catalysts, and excellent stability can greatly decrease the operational costs.[16] In CO_2ER, electrode stability not only requires resistance to deactivation, but also resistance to impurities.[17] The long-term operation of CO_2ER has been reported in several articles.[18] However, its resistance to impurities has not been widely covered. Again, taking the use of post-combustion gases from power plants as a CO_2 feedstock as an example, the post-combustion gas would contain a relatively high level of impurities, such as SO_x and NO_x, even after a primary treatment, and S has been identified having a harmful effect on many electrocata-

lysts.[19] Furthermore, the electrolyte is another potential source of impurities.[11c, 20] In this regard, more research into impurity-resistant electrodes is highly important. In addition, electrode stability should be separated from system stability. For instance, electrode clogging because of the formation of bicarbonate crystals during CO_2ER is not related to the electrode itself, but to the reactor system, and such should be solved through system engineering.

3. MOF-Related Catalysts for CO2ER
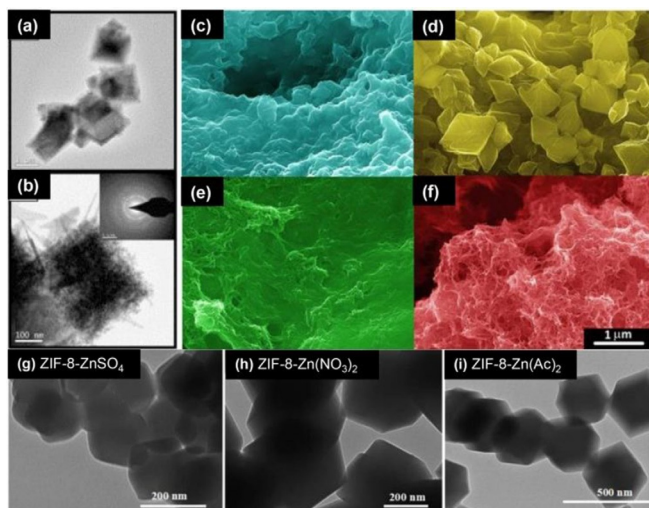
3.1. MOFs as Electrocatalysts

Metal–organic frameworks (MOFs), which combine the favorable characteristics of heterogeneous and homogeneous catalysts, have been explored as a new class of model catalytic material for understanding the electrochemical reduction of CO_2 (Table 1).

The application of MOF-related catalysts for the electrochemical reduction of CO_2 began in 2012,[21] when a copper rubeanate metal–organic framework (CR-MOF) was prepared by Hinogami et al. for the electrochemical reduction of CO_2 into valuable products (Figure 1). With an onset potential that was about 200 mV more positive than that of a copper electrode in the aqueous electrolyte, formic acid (HCOOH) was formed as

Table 1. Summary of the CO2ER performance of MOF-related materials.

Electrocatalyst[a]	Electrolyte	Main product	Peak FE[b] [%]	Peak j_{total} [mA cm^{-2}]	Peak potential[c] [V]
CR-MOF[21]	0.5 M KHCO$_3$	formic acid	ca. 100	7.1	−0.78
Cu-BTC[22]	0.01 M TBATFB in DMF	oxalic acid	ca. 51	19.22	−2.5 (vs. Ag/Ag$^+$)
ZIF-8[23]	0.5 M NaCl	CO	65	ca. 3	−1.14
ZIF-8[24]	0.25 M K$_2$SO$_4$	CO	81	8.5	−1.1
ZIF-108[24]	0.25 M K$_2$SO$_4$	CO	52	24.6	−1.3
Cu-BTC[25]	0.5 M KHCO$_3$	EtOH	10.3	10	−0.28
ligand-doped ZIF-8[26]	0.1 M KHCO$_3$	CO	90	10.1	−1.2
Re-MOF[27]	0.1 M TBAH in MeCN+5% TFE	CO	93	>2	−1.6 (vs. NHE)
ZIF-BTC[28]	BMIMBF$_4$	CH$_4$	80	3.1	−2.2 (vs. Ag/Ag$^+$)
Fe MOF-525[29]	1 M TBATF$_6$ in DMF	CO	50	ca. 6	−1.3 (vs. NHE)
PCN-222(Fe)[30]	0.5 M KHCO$_3$	CO	91	1.2	−0.6
Cu$_2$(CuTCPP) nanosheet[31]	MeCN with 1 M H$_2$O and 0.5 M EMIMBF$_4$	HCOO$^-$	68.4	ca. 4.5	−1.55 (vs. Ag/Ag$^+$)
Al$_2$(OH)$_2$TCPP-Co MOF[32]	0.5 M KHCO$_3$	CO	76	ca. 1	−0.7
Ag$_2$O/layered ZIF[33]	0.25 M K$_2$SO$_4$	CO	ca. 80	32	−1.3
Cu-SIM NU-1000[34]	0.1 M NaClO$_4$	HCOO$^-$	28	1.2	−0.82
Cu$_2$O@Cu-MOF[35]	0.1 M KHCO$_3$	CH$_4$	63.2	−14	−1.71
OD-Cu/C[36]	0.1 M KHCO$_3$	MeOH	ca. 43.2	ca. 8.9	−0.3
MOF-derived Cu NPs[37]	0.1 M KHCO$_3$	CH$_4$	ca. 50	7.5	−1.3
ZIF-8-derived Fe-N active sites[38]	1 M KHCO$_3$	CO	93	5.2	−0.43
Ni SA/N-C[39]	0.5 M KHCO$_3$	CO	71.9	10.48	−1.0
N-coordinated Fe[40]	0.1 M KHCO$_3$	CO	93	2.8	−0.58
Low-CN Cu clusters[41]	1 M KOH	C$_2$H$_4$	45	262	−1.07
N-coordinated Co[42]	0.5 M KHCO$_3$	CO	94	18.1	−0.63
MOF-derived In-Cu bimetallic oxides[43]	0.5 M KHCO$_3$	CO	92.1	11.2	−0.8
ZIF-8-derived NC[44]	0.1 M KHCO$_3$	CO	78	1.1	−0.93
ZIF-8-derived NC[45]	0.5 M KHCO$_3$	CO	95.4	1	−0.5
pyrolyzed ZIF/MWCNT[46]	0.1 M NaHCO$_3$	CO	100	7.7	−0.86

[a] The MOF-related catalysts mentioned in this table were used in a supporting manner. [b] Peak FE represents the FE value of the main product(s). [c] Peak potential represents the potential at which the peak FE occurs, and is versus the reversible hydrogen electrode (RHE) unless otherwise noted. CN = coordination number, TBATFB = tetrabutylammonium tetrafluoroborate, TBAH = tetrabutylammonium hydroxide, TFE = 2,2,2-trifluoroethanol, BMIM = 1-butyl-3-methylimidazolium, TBATF$_6$ = tetrabutylammonium hexafluorophosphate, EMIM = 1-ethyl-3-methylimidazolium.

Figure 1. Electron micrographs of MOFs that have been directly used as electrocatalysts: a) High- and b) low-magnification TEM images of Cu-BTC; inset shows the corresponding selected-area electron diffraction (SAED) pattern.[22] c–f) SEM images at ×25 000 magnification of HKUST-1 (c), Cu-AdeAce (d), Cu-DTA (e), and CuZn-DTA (f). The colors are for illustrative purposes only and do not represent the actual colors of the materials.[25] g–i) TEM images of ZIF-8-ZnSO$_4$ (g), ZIF-8-Zn(NO$_3$)$_2$ (h), and ZIF-8-Zn(AC)$_2$ (i).[23] AC = acetate.

almost the only CO$_2$-reduction product (FE ≈ 100 %), whereas several products were generated on a copper electrode. The partial current of HCOOH for the CR-MOF electrode was about 7.1 mA cm^{-2}, which was also higher than for the copper electrode, around 0.55 mA cm^{-2}.

Also in 2012, Senthil Kumar et al. reported cyclic voltammetry (CV) studies of copper benzene-1,3,5-tricarboxylate (Cu-BTC) films on glassy carbon electrodes in 0.1 M KCl.[22] Well-defined Cu^{II}/Cu^{I} and Cu^{I}/Cu^{0} reversible redox responses were observed, and the MOF film was subsequently studied as an electrocatalyst in DMF. The production of oxalic acid was confirmed by GC-MS, with a Faradaic efficiency of about 51 % and a total current density of 19 mA cm^{-2}.

Following these pioneering works, several other MOF-based catalysts have been investigated in the CO$_2$ER. Zeolitic imidazolate framework ZIF-8, an archetypical MOF material, was synthesized from a variety of zinc sources by Wang et al. and used as an electrocatalyst for the reduction of CO$_2$ into CO.[23] ZIF-8 that was prepared from ZnSO$_4$ delivered the best catalytic activity, with a Faradaic efficiency towards CO of FE$_{CO}$ = 65 % and a total current density of j_{total} ≈ 3 mA cm^{-2}, thereby establishing a relationship between CO$_2$ER performance and the synthetic zinc source. The main catalytic active sites were claimed to be the discrete zinc nodes in ZIF-8.

Jiang et al. further identified the imidazolate ligands that were coordinated to the zinc(II) center in the ZIFs as the catalytic sites for CO$_2$ER with the help of in situ X-ray absorption spectroscopy (XAS) measurements and DFT calculations.[24] They investigated a range of ZIFs that exhibited the same sodalite topology but with different organic ligands, including ZIF-8, ZIF-108, ZIF-7, and substituted imidazolate material SIM-1, for the CO$_2$ER in aqueous electrolyte. Of the ZIF catalysts

that were tested, ZIF-8 showed the highest FE$_{CO}$ of 81.0 % at −1.1 V (vs. RHE), whilst ZIF-108 showed the highest maximum CO current density of 12.8 mA cm^{-2} at −1.3 V (vs. RHE).

The effect of the linker on the CO$_2$ER was also investigated by Albo et al.[25] Thus, four copper-based MOFs, namely, Cu-BTC (HKUST-1), copper(II) adeninate acetate (Cu-AdeAce), copper bisbidentate dithiooxamidate (Cu-DTA) mesoporous metal–organic aerogel (MOA), and CuZn-DTA MOA, were synthesized and supported on gas-diffusion electrodes. The MOF-based electrodes all showed electrocatalytic efficiency for the production of MeOH and EtOH in the liquid phase. The Cu-BTC-based electrode showed the highest cumulative FE for CO$_2$ conversion of 15.9 % at a current density of 10 mA cm^{-2}. It was found that MOFs that contained coordinately unsaturated metal sites were favorable for the enhancement of the electrocatalytic reduction of CO$_2$ into alcohols. Furthermore, Cu-BTC-based electrodes showed stable electrocatalytic performance for 17 h.

In addition to structural effects, the linker in the MOFs can also be functionalized to boost the catalytic activity. The poor conductivity of MOFs largely hinders their direct application as electrocatalysts. Thus, Dou et al. reported a general strategy for ligand doping to enhance charge transfer, thereby improving the electrocatalytic activity.[26] A strongly electron-donating molecule, 1,10-phenanthroline, was introduced into ZIF-8 as a CO$_2$-reduction electrocatalyst. Experimental and theoretical results suggested that the electron-donating nature of 1,10-phenanthroline enabled charge transfer, which facilitated the generation of ˙COOH. As a consequence, the ligand-doped ZIF-8 showed an FE$_{CO}$ of 90 % and j_{total} of 10.1 mA cm^{-2}, both of which were significantly improved compared with pristine ZIF-8.

Ye et al. deposited a highly oriented monolithic rhenium-based MOF thin film onto a conductive fluorine-doped tin oxide (FTO) electrode by using liquid-phase epitaxy.[27] The MOF film was exclusively grown along the [001] direction, and exhibited a high FE$_{CO}$ of about 93 % when operated as an electrocatalyst for the reduction of CO$_2$, with a current density in excess of 2 mA cm^{-2}.

As discussed above, overpotential is one of the key issues that need to be addressed in the CO$_2$ER. Kang et al. employed the combination of an ionic liquid (IL) as an electrolyte and Zn-BTC as a catalyst as a strategy to lower the overpotential in the CO$_2$ER,[28] which represented the first combination of a MOF electrode and a pure IL electrolyte in this field. The Zn-BTC electrode showed a higher selectivity for CH$_4$ (> 80 %) and higher current density (3 mA cm^{-2}) at mild overpotentials (250 mV) than the commonly used metal electrodes.

3.2. MOFs as Active-Phase Supports

In addition to their direct application as electrocatalysts, the unique textural properties of MOFs also offer a number of opportunities for their application as active-phase supports for the CO$_2$ER (Figure 2).

Porphyrin-based molecular catalysts have been widely used in the CO$_2$ER.[47] The significance of molecular-catalyst immobi-
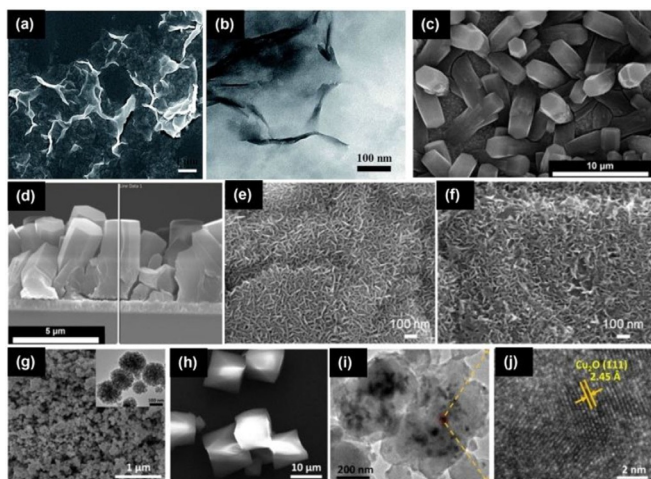
Figure 2. Electron micrographs of MOFs that have been used as catalyst supports: a) SEM and b) TEM images of $Cu_2(CuTCPP)$ nanosheets.[31] c) Top-down and d) cross-sectional SEM images of a Cu-SIM NU-1000 thin film.[34] e, f) SEM images of the MOF catalyst film before (e) and after electrolysis (f), which revealed the retention of the plate-like morphology.[32] g) SEM image of Cu_2O spheres; inset shows the corresponding TEM image. h) SEM image of Cu-MOF. i) TEM and j) HRTEM images of $Cu_2O@Cu$-MOF after reacting for 12 h.[35]

lization was highlighted by Hu et al., by comparing the performance of cobalt meso-tetraphenylporphyrin (CoTPP) under both supported and unsupported conditions.[48] CoTPP performed poorly as a homogeneous electrocatalyst, thereby giving low product selectivity at a high overpotential, whereas a remarkable enhancement in catalytic activity was observed upon directly immobilizing CoTPP onto carbon nanotubes, with the selective formation of CO ($>90\%$) at a low overpotential. Kramer and McCrory demonstrated that the immobilization agent had an effect on the molecular catalyst's performance, by comparing the CO_2ER activities of cobalt phthalocyanine (CoPc) that was supported on edge-plane graphite and poly-4-vinylpridine (P4VP) thin films.[49] CoPc that was embedded in the P4VP matrix displayed improved FE_{CO} and turnover frequency, which was attributed to the chemical coordination environment that was provided by the P4VP polymer matrix.

Hod et al. used iron porphyrin as a CO_2-reduction catalyst, which was incorporated into MOF-525 as both a structural and functional component.[29] First, MOF-525 was deposited onto a conductive indium tin oxide (ITO) substrate, and then the iron porphyrin was formed by using a post-metalation strategy. This approach led to a high surface coverage of electrochemically addressable iron porphyrin sites (ca. 1015 sites cm^{-2}), with the formation of a roughly equal mixture of CO and H_2 ($FE_{CO} \approx 50\%$) as products and a j_{total} of 6 mA cm^{-2}. Despite the low FE, these results demonstrated that porphyrins could be electrochemically accessed when incorporated into a MOF structure.

Electroactive porphyrins can also be used as ligands to form MOFs. Dong et al. rationally introduced an iron tetrakis(4-carboxyphenyl)porphyrin (Fe-TCPP) to form a porous coordination network, PCN-222(Fe), for use as a CO_2ER catalyst.[30] After dip-coating onto a carbon substrate, the composite catalyst PCN-

222(Fe)/C (mass ratio $= 1:2$) exhibited a maximum FE_{CO} of 91%, with an overpotential of 494 mV ($j_{total} = 1.2$ mA cm^{-2}) in aqueous solution, thereby achieving a turnover frequency (TOF) of 0.336 sites^{-1} s^{-1}. The catalyst was found to retain its crystallinity and stability after 10 hours of electrolysis at -0.60 V (vs. RHE; average $FE_{CO} = 80.4\%$).

Wu et al. used porphyrinic MOF nanosheets to promote the CO_2ER.[31] The $Cu_2(CuTCPP)$ nanosheets were cathodized onto FTO glass and exhibited significant activity for the production of formate, with a FE of 68.4% at -1.55 V (vs. Ag/Ag^+). Moreover, the C–C-coupling product (acetate) was also formed from the same catalyst within the voltage range 1.40–1.65 V, with a total liquid product FE of 38.8–85.2%. Characterization results revealed the instability of $Cu_2(CuTCPP)$, with the transformation of Cu^{II} into CuO, Cu_2O, and Cu_4O_3, which significantly catalyzed the conversion of CO_2 into formate and acetate.

Kornienko et al. employed an aluminum-porphyrin-based MOF, MOF-55,[32] which comprised cobalt porphyrin active sites, for the electrocatalytic reduction of CO_2 into CO. First, a thin film of aluminum oxide was deposited by using atomic layer deposition (ALD) as a metal precursor. Subsequent MOF formation proceeded through the reaction of the coated aluminum oxide with the linker under solvothermal conditions. The thickness of the precursor could be easily controlled by tuning the number of ALD cycles, thereby controlling the thickness of the catalyst layers. The performance of the resulting MOF catalyst initially improved with increasing film thickness to a maximum of about 2.8 mA cm^{-2}. This appearance of a performance maximum possibly indicated a trade-off between electron and mass transport. The optimized catalyst thickness exhibited FE_{CO} production of up to 76% in a 7 hour test.

In addition to molecular catalysts, MOFs have also been used to support metal nanoparticles in the CO_2ER. Jiang et al. reported the construction of a Ag_2O/layered-ZIF composite structure by mixing pre-synthesized layered ZIF-7 with an aqueous solution of $AgNO_3$, followed by heating at reflux (100 °C).[33] The Ag_2O/layered-ZIF composite showed much higher FE_{CO} (ca. 80%) and j_{CO} (ca. 32 mA cm^{-2}) values than the layered ZIF or Ag/C alone. This performance enhancement was attributed to a synergistic effect between the Ag_2O nanoparticles and the layered ZIF, as well as to the facilitation of mass transport by the high specific surface area in the composite.

Kung et al. embedded copper nanoparticles into thin films of NU-1000 by first installing single-site copper(II) into the NU-1000 thin film, followed by electrochemical reduction into metallic copper.[34] The copper nanoparticles were electrochemically addressable and exhibited moderate electrocatalytic activity, with a maximum FE for $HCOO^-$ of 28% and -1.2 mA cm^{-2} at -0.82 V (vs. RHE). Both the crystallinity and morphology of the thin film remained unchanged after electrocatalysis. The authors also found that the particle size was largely dependent on the pore size of the MOF, which might offer an opportunity to achieve tunable catalyst sizes through this pore-confinement effect.

In a recent study, Tan et al. synthesized a tailor-made $Cu_2O@Cu$-MOF electrocatalyst through the in situ etching of

Cu_2O spheres with H3BTC to form a Cu-MOF shell.[35] The as-prepared electrocatalyst exhibited intriguing performance for the formation of hydrocarbons from CO_2, with a high FE for CH_4 and C_2H_4 of 79.4%, and especially a FE for CH_4 of up to 63.2% at -1.71 V.

3.3. MOFs as Electrocatalyst Precursors

Although quite a few reports in which MOFs have been used directly as catalysts have claimed that the MOF catalysts showed good stability during testing, a lot of them failed to conduct post-reaction analysis to confirm these statements.[50] Indeed, stability is a serious issue for MOFs, in particular under the highly negative potentials that are usually required in the CO_2ER, because these potentials are often more negative than the reduction potentials of many metals that are used in the MOF synthesis (Table 2). In this spirit, the use of a MOF as a catalyst precursor can be a favorable way of producing a stable and efficient catalyst (Figure 3).

The decomposition of MOFs under controlled conditions typically leads to the clustering of its metal component into small nanoparticles. Zhao et al. synthesized oxide-derived copper/carbon (OD Cu/C) catalysts through facile carbonization of the MOF Cu-BTC (HKUST-1).[36] The resulting materials promoted a highly selective reduction of CO_2 into alcohols, with a total FE of 71.2% at -0.7 V (vs. RHE). High yields of MeOH and EtOH were achieved on OD Cu/C-1000, with peak production rates of 12.4 $mg\,L^{-1}\,h^{-1}$ at -0.3 V and 13.4 $mg\,L^{-1}\,h^{-1}$ at -0.7 V, respectively. Notably, the onset potential for EtOH formation was among the lowest overpotentials reported to date for the reduction of CO_2 into EtOH. This improvement in the activity and selectivity of the oxide-derived Cu/C were attributed to a synergistic effect between the highly dispersed copper and the matrix of porous carbon.

Kim et al. employed an electrochemical reduction strategy for the decomposition of MOFs, thereby obtaining an efficient
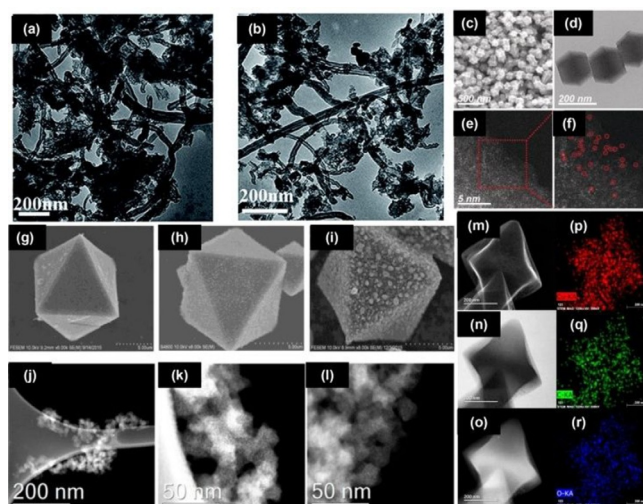
Figure 3. Electron micrographs of MOFs that have been used as catalyst precursors: a, b) TEM images of ZIF-CNT-FA-p (a) and ZIF-Fe-CNT-FA-p (b).[46] c) SEM and d) TEM images of N-coordinated Co. e, f) Magnified high-angle annular dark-field–scanning transmission electron microscopy (HAADF-STEM) images of N-coordinated Co, which show the atomic dispersion of the Co atoms.[42] g–i) SEM images of OD-Cu/C materials that had been processed at different temperatures.[36] j–l) HAADF-STEM images of Fe-N-C.[40] m–r) Structural investigation of as-fabricated HKUST-1 by using SEM (m), bright-field TEM (n), HAADF TEM (o), and energy-dispersive X-ray spectroscopy TEM (EDS TEM; p–r).[41]

electrocatalyst for the synthesis of CH_4.[37] They chose copper-based MOF-74 as the precursor, which was electrochemically reduced into copper nanoparticles (NPs). The porous structure of the MOF served as a template for the synthesis of isolated Cu NPs with high current densities and a high FE for CH_4 in the electrochemical reduction of CO_2. The MOF-derived Cu NPs resulted in a FE_{CH_4} of >50% and a 2.3-fold-higher current density at -1.3 V (vs. RHE) than that of commercially available Cu NPs.

Besides metal nanoparticles, MOF-mediated synthesis can also act as an effective method for generating isolated metal–nitrogen sites with a high degree of exposure of the active sites for efficient catalysis. Ye et al. fabricated isolated iron–nitrogen sites on the surface of a carbon matrix through the pyrolysis of ammonium ferric citrate (AFC)/ZIF-8 composites.[38] The AFC/ZIF-8 composite was synthesized by reacting a solution of the zinc precursor and AFC with a solution of 2-methylimidazole, followed by cleaning, centrifugation, and drying. The highly exposed iron–nitrogen sites demonstrated high selectivity for CO (maximum $FE_{CO}=93\%$) and high activity ($j_{CO}=9.5$ $mA\,cm^{-2}$).

Zhao et al. employed nickel-ion-exchanged ZIF-8 to assist in the preparation of a catalyst that contained single nickel sites for the efficient electroreduction of CO_2.[39] Their synthesis was based on an inexpensive ion exchange between zinc nodes and adsorbed nickel ions within the cavities of the MOF, followed by pyrolysis of the ion-exchanged MOF. This single-atom catalyst exhibited an outstanding turnover frequency for the electroreduction of CO_2 (5273 h^{-1}), with a FE_{CO} of over 71.9% and a j_{total} of 10.48 $mA\,cm^{-2}$ at an overpotential of 890 mV.

Table 2. Standard electrode potentials of common metal nodes in MOFs.[51]

Half reaction	Potential [V vs. RHE]
$Co^{3+}+e^-\rightleftharpoons Co^{2+}$	1.82
$Ag^++e^-\rightleftharpoons Ag$	0.8
$Fe^{3+}+e^-\rightleftharpoons Fe^{2+}$	0.77
$Cu^++e^-\rightleftharpoons Cu$	0.52
$O_2+2H_2O+4e^-\rightleftharpoons 4OH^-$	0.4
$Cu^{2+}+2e^-\rightleftharpoons Cu$	0.34
$Cu^{2+}+e^-\rightleftharpoons Cu^+$	0.15
$2H^++2e^-\rightleftharpoons H_2$	0
$Fe^{3+}+3e^-\rightleftharpoons Fe$	-0.04
$Ni^{2+}+2e^-\rightleftharpoons Ni$	-0.25
$Co^{2+}+2e^-\rightleftharpoons Co$	-0.29
$Fe^{2+}+2e^-\rightleftharpoons Fe$	-0.41
$Cr^{3+}+e^-\rightleftharpoons Cr^{2+}$	-0.42
$Cr^{3+}+3e^-\rightleftharpoons Cr$	-0.74
$Zn^{2+}+2e^-\rightleftharpoons Zn$	-0.76
$Ti^{3+}+3e^-\rightleftharpoons Ti$	-1.37
$Zr^{4+}+4e^-\rightleftharpoons Zr$	-1.45
$Ti^{2+}+2e^-\rightleftharpoons Ti$	-1.63
$Al^{3+}+3e^-\rightleftharpoons Al$	-1.66

Pan et al. studied the structure and reactivity of atomically dispersed M-N_4 (M=Fe, Co) single sites in the CO_2ER. Nitrogen-coordinated iron or cobalt single sites that were atomically dispersed within a carbon matrix (M-N-C) were prepared by using MOF precursors, and were further studied as model catalysts.[40] Iron was found to be intrinsically more active than cobalt in M-N_4 for the reduction of CO_2 into CO in terms of a higher FE_{CO} (93% vs. 45%) and current density. Computations based on first principles elucidated that the M-N_{2+2}-C_8 moieties, which were distributed at the edge of the carbon matrix and bridged two adjacent armchair-like graphitic layers, were the active sites for the CO_2ER.

Selectivity is one of the key issues that face the CO_2ER, in particular when copper-based catalysts are used. Nam et al. reported a strategy that involved the formation of MOF-regulated copper clusters, which shifted the electroreduction of CO_2 towards multiple-carbon-atom-containing products.[41] The symmetrical "paddle-wheel" copper dimer, the secondary building block of HKUST-1, was distorted into an asymmetric motif by separating adjacent benzene tricarboxylate moieties under thermal treatment. By varying the processing conditions, the asymmetrical local atomic structure, oxidation state, and bonding strain in the copper dimers were modulated. The formation of copper clusters with low coordination numbers from distorted copper dimers in HKUST-1 was observed during the electroreduction of CO_2, thus leading to a Faradaic efficiency for C_2H_4 of 45%. This enhanced performance was closely related to maintaining a low Cu—Cu coordination number among the copper clusters during the reaction.

Another example of regulating coordination number to tune the selectivity was reported by Wang et al.[42] They prepared a series of atomically dispersed cobalt catalysts with different nitrogen-coordination numbers for the CO_2ER. The best catalyst, which contained atomically dispersed cobalt moieties with two-coordinate nitrogen atoms, achieved both high selectivity (FE_{CO}=94%) and superior activity (j_{total}=18.1 mA cm^{-2}) at an overpotential of 520 mV. The turnover frequency for CO formation reached a record value of 18 200 h^{-1}. These results demonstrated that a lower coordination number facilitated the activation of CO_2 to form the $\cdot$COO$^-$ intermediate and, hence, enhance the CO_2ER activity.

Very recently, Guo et al. introduced a new method to tune the selectivity of the CO_2ER by using a MOF-derived bimetallic oxide catalyst.[43] Thus, MOF-derived In-Cu bimetallic oxides were synthesized through the pyrolysis of an In-Cu bimetallic MOF. By controlling the indium/copper ratio, the FE_{CO} value could reach as high as 92.1%, along with a j_{total} of 11.2 mA cm^{-2}. This excellent performance was mainly attributed to stronger CO_2 adsorption, higher electrochemical surface area, and lower charge-transfer resistance by the bimetallic catalyst.

Besides metal-based catalysts, the use of a carbon-rich organic linker, in combination with the low boiling point of some metal nodes, such as zinc, renders MOFs as promising precursors for the production of carbon-based electrocatalysts.[52] Following this strategy, Wang et al. synthesized a nitrogen-doped carbon (NC) material through the pyrolysis of the well-known metal–organic framework ZIF-8.[44] The resulting NC-based CO_2ER electrode showed Faradaic efficiencies as high as $FE_{CO}\approx78\%$. The authors also found that the pyrolysis temperature determined the amount and the accessibility of nitrogen species in the carbon electrode, in which pyridinic-N and quaternary-N species played key roles in the selective formation of CO. In general, materials that are derived from zinc-based ZIFs are nothing less than nitrogen-containing carbon materials and are active without the addition of other metals. Therefore, it should be kept in mind to benchmark their performance against those materials that were prepared through other routes.[53]

The effect of pyrolysis temperature and the mechanism of the ZIF-8-derived NC were further studied by Zheng et al.[45] They prepared NC catalysts by decomposing ZIF-8 at different temperatures under an argon atmosphere. They found that higher pyrolysis temperatures led to better CO_2ER activity. The NC catalyst with the best performance exhibited high selectivity, with 95.4% FE_{CO} at −0.5 V (vs. RHE). This catalyst also maintained stability during operation for 20 hours, after which the FE_{CO} was still greater than 90%. Their experiments showed that a higher pyrolysis temperature decreased the total nitrogen content, but changed the nature and density of the nitrogen species. DFT calculations revealed that higher pyrolysis temperatures led to enhanced activity by promoting the formation of pyridinic N species, which provided more efficient active sites.

To relieve the limits on electron transportation with the MOF-mediated approach, Guo et al. synthesized a composite material through the copyrolysis of in-situ-grown ZIF-8 on a multiwalled carbon nanotubes (MWCNTs) substrate.[46] This composite selectively catalyzed the electrochemical reduction of CO_2 into CO in aqueous solution with FE$\approx$100% and a current density of up to 7.7 mA cm^{-2} at an overpotential of 740 mV. By comparison, pyrolyzed ZIF-8 without the MWCNTs only showed a FE_{CO} of about 50%. The addition of iron to the ZIF lowered the overpotential, but also changed the selectivity. The MWCNT support was crucial to achieving superior efficiency, by enhancing electron transport through the MWCNT network and simultaneously expediting the CO_2 transport in the mesoporous structure that was formed by the MWCNTs.

4. Concluding Remarks

The CO_2ER is widely regarded as one of the most promising technologies for solving the global problem of CO_2 emissions, although it still faces several challenges on the path toward commercialization. Herein, we have summarized recent works on the electroreduction of CO_2 that use MOF and MOF-mediated catalysts. Generally speaking, the main advantages of MOFs in the CO_2ER originate from their unique textural and structural properties. When MOFs are directly used as catalysts, the atomically dispersed metal nodes can offer highly active sites, and the organic linkers can also be modified into catalytic sites or charge-transfer agents. Their porous structure, which is formed by the metal nodes and organic linkers, makes catalytic sites more accessible to CO_2 if the catalysis takes place on the

MOF itself or on supported species. Moreover, the compatibility of MOFs with ILs facilitates their application in this medium. The use of MOFs as catalyst precursors typically leads to highly dispersed metal particles or carbon-based catalysts, thereby maximizing catalyst utilization. The homogeneously dispersed metal sites can be inherited by the MOF-derived catalysts to form efficient single-site catalysts with unprecedented TOFs, and the highly tunable building blocks of MOFs enable the formation of bimetallic structures, which provide a facile route for the synthesis of metal alloys, thereby opening the door to breaking scaling relationships in the CO_2ER.[10]

Although remarkable results have been reported with MOF-related catalysts, there are still several issues that need to be carefully addressed in future research. Stability is one of the most concerning issues facing the CO_2ER. Whilst most authors have claimed that pristine MOFs that are based on readily reducible metals are stable under CO_2ER reaction conditions, catalyst stability has only been confirmed in a few cases by using post-analysis characterization.[30, 32, 34, 35] Herein, we would like to clarify that the stability of the crystalline MOF does not necessarily need to be an issue. Indeed, from an application point of view, the electrochemical reduction of MOFs to form small metal nanoparticles may render very interesting catalytic systems. However, as scientists, we should make sure that we do not jump to the wrong conclusions by attributing the observed catalytic performance to the MOF scaffold.

As is the case in thermal catalysis, probably the most exciting results in terms of performance have been reported for MOF-derived catalysts.[7a, 54] We believe that this route offers great possibilities for the further engineering of CO_2ER catalysts and for the optimization of metal use in catalysis, an aspect that may become critical if CO_2 electrolyzers are applied on a mass scale.

Last, but not least, it is fair to admit that, so far, most of the catalytic results have been achieved by using aqueous electrolytes in semi-batch experiments, whilst only low current densities have been achieved, owing to the low solubility of CO_2 in the aqueous phase. We are sure that, as is already happening for "traditional" electrocatalysts, MOF-derived systems will soon be tested under more commercially relevant conditions by making use of gas-diffusion electrochemical cells, in which high current densities (>100 mA cm^{-2}) have been achieved.[55] By using carbon-capture technologies from point sources, liquid CO_2 will become available at pressures exceeding 100 bar and its solubility may stop being a limiting factor. Also, aspects of molecular and electron transport require careful attention, as shown by Guo et al.[46]

Overall, we are confident that MOF-related catalyst engineering, when combined with systems integration in the CO_2ER, will mark a substantial contribution to the field of electrocatalytic CO_2 reduction.

Acknowledgements

Conflict of interest

The authors declare no conflict of interest.

[1] C. Chen, J. F. K. Kotyk, S. W. Sheehan, *Chem* **2018**, *4*, 2571–2586.
[2] A. Dokania, A. Ramirez, A. Bavykina, J. Gascon, *ACS Energy Lett.* **2019**, *4*, 167–176.
[3] Y. Hori in *Handbook of Fuel Cells: Fundamentals, Technology, and Applications* (Eds.: W. Vielstich, A. Lamm, H. A. Gasteiger, H. Yokokawa), Wiley, Hoboken, NJ, **2010**, "CO2-Reduction, Catalyzed by Metal Electrodes".
[4] a) D. Gao, F. Cai, G. Wang, X. Bao, *Curr. Opin. Green Sustainable Chem.* **2017**, *3*, 39–44; b) M. Ma, W. A. Smith in *Anisotropic and Shape-Selective Nanomaterials: Structure-Property Relationships* (Eds.: S. E. Hunyadi Murph, G. K. Larsen, K. J. Coopersmith), Springer International Publishing, Cham, **2017**, pp. 337–373; c) L. Zhang, Z.-J. Zhao, J. Gong, *Angew. Chem. Int. Ed.* **2017**, *56*, 11326–11353; *Angew. Chem.* **2017**, *129*, 11482–11511.
[5] a) A. Corma, H. García, F. X. Llabrés i Xamena, *Chem. Rev.* **2010**, *110*, 4606–4655; b) A. U. Czaja, N. Trukhan, U. Müller, *Chem. Soc. Rev.* **2009**, *38*, 1284–1293; c) A. Dhakshinamoorthy, H. Garcia, *Chem. Soc. Rev.* **2012**, *41*, 5262–5284; d) D. Farrusseng, S. Aguado, C. Pinel, *Angew. Chem. Int. Ed.* **2009**, *48*, 7502–7513; *Angew. Chem.* **2009**, *121*, 7638–7649; e) D. Feng, Z.-Y. Gu, J.-R. Li, H.-L. Jiang, Z. Wei, H.-C. Zhou, *Angew. Chem. Int. Ed.* **2012**, *51*, 10307–10310; *Angew. Chem.* **2012**, *124*, 10453–10456; f) H. Furukawa, K. E. Cordova, M. O'Keeffe, O. M. Yaghi, *Science* **2013**, *341*, 1230444; g) S. L. James, *Chem. Soc. Rev.* **2003**, *32*, 276–288; h) J. Lee, O. K. Farha, J. Roberts, K. A. Scheidt, S. T. Nguyen, J. T. Hupp, *Chem. Soc. Rev.* **2009**, *38*, 1450–1459; i) J. Liu, L. Chen, H. Cui, J. Zhang, L. Zhang, C.-Y. Su, *Chem. Soc. Rev.* **2014**, *43*, 6011–6061; j) Y. Liu, W. Xuan, Y. Cui, *Adv. Mater.* **2010**, *22*, 4112–4135; k) L. Ma, C. Abney, W. Lin, *Chem. Soc. Rev.* **2009**, *38*, 1248–1256; l) L. Ma, J. M. Falkowski, C. Abney, W. Lin, *Nat. Chem.* **2010**, *2*, 838; m) K. Schlichte, T. Kratzke, S. Kaskel, *Microporous Mesoporous Mater.* **2004**, *73*, 81–88; n) J. S. Seo, D. Whang, H. Lee, S. I. Jun, J. Oh, Y. J. Jeon, K. Kim, *Nature* **2000**, *404*, 982–986; o) C.-D. Wu, A. Hu, L. Zhang, W. Lin, *J. Am. Chem. Soc.* **2005**, *127*, 8940–8941; p) H.-C. Zhou, J. R. Long, O. M. Yaghi, *Chem. Rev.* **2012**, *112*, 673–674; q) L. Alaerts, E. Séguin, H. Poelman, F. Thibault-Starzyk, P. A. Jacobs, D. E. De Vos, *Chem. Eur. J.* **2006**, *12*, 7353–7363; r) M. H. Alkordi, Y. Liu, R. W. Larsen, J. F. Eubank, M. Eddaoudi, *J. Am. Chem. Soc.* **2008**, *130*, 12639–12641; s) S.-H. Cho, B. Ma, S. T. Nguyen, J. T. Hupp, T. E. Albrecht-Schmitt, *Chem. Commun.* **2006**, 2563–2565; t) D. Dang, P. Wu, C. He, Z. Xie, C. Duan, *J. Am. Chem. Soc.* **2010**, *132*, 14321–14323; u) A. Dhakshinamoorthy, M. Alvaro, H. Garcia, *Catal. Sci. Technol.* **2011**, *1*, 856–867; v) A. Dhakshinamoorthy, M. Alvaro, H. Garcia, *Chem. Commun.* **2012**, *48*, 11275–11288; w) A. Dhakshinamoorthy, H. Garcia, *Chem. Soc. Rev.* **2014**, *43*, 5750–5765; x) J. Gascon, U. Aktay, M. D. Hernandez-Alonso, G. P. M. van Klink, F. Kapteijn, *J. Catal.* **2009**, *261*, 75–87; y) S. Horike, M. Dincă, K. Tamaki, J. R. Long, *J. Am. Chem. Soc.* **2008**, *130*, 5854–5855; z) A. J. Howarth, Y. Liu, P. Li, Z. Li, T. C. Wang, J. T. Hupp, O. K. Farha, *Nat. Rev. Mater.* **2016**, *1*, 15018; aa) Y.-B. Huang, J. Liang, X.-S. Wang, R. Cao, *Chem. Soc. Rev.* **2017**, *46*, 126–157; ab) H.-L. Jiang, T. Akita, T. Ishida, M. Haruta, Q. Xu, *J. Am. Chem. Soc.* **2011**, *133*, 1304–1306; ac) U. Mueller, M. Schubert, F. Teich, H. Puetter, K. Schierle-Arndt, J. Pastré, *J. Mater. Chem.* **2006**, *16*, 626–636; ad) M. Ranocchiari, J. A. van Bokhoven, *Phys. Chem. Chem. Phys.* **2011**, *13*, 6388–6396; ae) F. Song, C. Wang, J. M. Falkowski, L. Ma, W. Lin, *J. Am. Chem. Soc.* **2010**, *132*, 15390–15398; af) C.-Y. Sun, S.-X. Liu, D.-D. Liang, K.-Z. Shao, Y.-H. Ren, Z.-M. Su, *J. Am. Chem. Soc.* **2009**, *131*, 1883–1888; ag) P. Valvekens, F. Vermoortele, D. De Vos, *Catal. Sci. Technol.* **2013**, *3*, 1435–1445; ah) F. Vermoortele, B. Bueken, G. Le Bars, B. Van de Voorde, M. Vandichel, K. Houthoofd, A. Vimont, M. Daturi, M. Waroquier, V. Van Speybroeck, C. Kirschhock, D. E. De Vos, *J. Am. Chem. Soc.* **2013**, *135*, 11465–11468; ai) C.-D. Wu, W. Lin, *Angew. Chem. Int. Ed.* **2007**, *46*, 1075–1078; *Angew. Chem.* **2007**, *119*, 1093–1096; aj) Q. Yang, Q. Xu, H.-L. Jiang, *Chem. Soc. Rev.* **2017**, *46*, 4774–4808; ak) M. Zhao, K. Deng, L. He, Y. Liu, G. Li, H.

Zhao, Z. Tang, *J. Am. Chem. Soc.* **2014**, *136*, 1738–1741; al) L. Zhu, X.-Q. Liu, H.-L. Jiang, L.-B. Sun, *Chem. Rev.* **2017**, *117*, 8129–8176; am) Q.-L. Zhu, J. Li, Q. Xu, *J. Am. Chem. Soc.* **2013**, *135*, 10210–10213; an) R.-Q. Zou, H. Sakurai, Q. Xu, *Angew. Chem. Int. Ed.* **2006**, *45*, 2542–2546; *Angew. Chem.* **2006**, *118*, 2604–2608.

[6] a) J. Gascon, A. Corma, F. Kapteijn, F. X. Llabrés i Xamena, *ACS Catal.* **2014**, *4*, 361–378; b) S. M. J. Rogge, A. Bavykina, J. Hajek, H. Garcia, A. I. Olivos-Suarez, A. Sepúlveda-Escribano, A. Vimont, G. Clet, P. Bazin, F. Kapteijn, M. Daturi, E. V. Ramos-Fernandez, F. X. Llabrés i Xamena, V. Van Speybroeck, J. Gascon, *Chem. Soc. Rev.* **2017**, *46*, 3134–3184.

[7] a) L. Oar-Arteta, T. Wezendonk, X. Sun, F. Kapteijn, J. Gascon, *Mater. Chem. Front.* **2017**, *1*, 1709–1745; b) V. P. Santos, T. A. Wezendonk, J. J. D. Jaén, A. I. Dugulan, M. A. Nasalevich, H.-U. Islam, A. Chojecki, S. Sartipi, X. Sun, A. A. Hakeem, A. C. J. Koeken, M. Ruitenbeek, T. Davidian, G. R. Meima, G. Sankar, F. Kapteijn, M. Makkee, J. Gascon, *Nat. Commun.* **2015**, *6*, 6451; c) X. Sun, A. I. Olivos-Suarez, L. Oar-Arteta, E. Rozhko, D. Osadchii, A. Bavykina, F. Kapteijn, J. Gascon, *ChemCatChem* **2017**, *9*, 1854–1862; d) X. Sun, A. I. O. Suarez, M. Meijerink, T. van Deelen, S. Ould-Chikh, J. Zečević, K. P. de Jong, F. Kapteijn, J. Gascon, *Nat. Commun.* **2017**, *8*, 1680.

[8] X. Sun, A. I. Olivos-Suarez, D. Osadchii, M. J. V. Romero, F. Kapteijn, J. Gascon, *J. Catal.* **2018**, *357*, 20–28.

[9] W. Xia, A. Mahmood, R. Q. Zou, Q. Xu, *Energy Environ. Sci.* **2015**, *8*, 1837–1866.

[10] R. Kortlever, J. Shen, K. J. Schouten, F. Calle-Vallejo, M. T. Koper, *J. Phys. Chem. Lett.* **2015**, *6*, 4073–4082.

[11] a) Q. Lu, F. Jiao, *Nano Energy* **2016**, *29*, 439–456; b) H. R. Jhong, S. C. Ma, P. J. A. Kenis, *Curr. Opin. Chem. Eng.* **2013**, *2*, 191–199; c) J.-P. Jones, G. K. S. Prakash, G. A. Olah, *Isr. J. Chem.* **2014**, *54*, 1451–1466; d) X. Lu, Y. Wu, X. Yuan, L. Huang, Z. Wu, J. Xuan, Y. Wang, H. Wang, *ACS Energy Lett.* **2018**, *3*, 2527–2532; e) X. Liu, J. Xiao, H. Peng, X. Hong, K. Chan, J. K. Nørskov, *Nat. Commun.* **2017**, *8*, 15438.

[12] a) S. Gonen, L. Elbaz, *Curr. Opin. Electrochem.* **2018**, *9*, 179–188; b) C. Kim, F. Dionigi, V. Beermann, X. Wang, T. Moller, P. Strasser, *Adv. Mater.* **2018**, 1805617; c) Y. Kim, A. Jo, Y. Ha, Y. Lee, D. Lee, Y. Lee, C. Lee, *Electroanalysis* **2018**, *30*, 2861–2868.

[13] B. Mondal, P. Sen, A. Rana, D. Saha, P. Das, A. Dey, *ACS Catal.* **2019**, *9*, 3895–3899.

[14] A. V. Rudnev, Y. C. Fu, I. Gjuroski, F. Stricker, J. Furrer, N. Kovacs, S. Vesztergom, P. Broekmann, *ChemPhysChem* **2017**, *18*, 3153–3162.

[15] L. Han, W. Zhou, C. Xiang, *ACS Energy Lett.* **2018**, *3*, 855–860.

[16] M. Rumayor, A. Dominguez-Ramos, A. Irabien, *Sustainable Prod. Consumpt.* **2019**, *18*, 72–82.

[17] Y. Hori, H. Konishi, T. Futamura, A. Murata, O. Koga, H. Sakurai, K. Oguma, *Electrochim. Acta* **2005**, *50*, 5354–5369.

[18] a) H. Won da, H. Shin, J. Koh, J. Chung, H. S. Lee, H. Kim, S. I. Woo, *Angew. Chem. Int. Ed.* **2016**, *55*, 9297–9300; *Angew. Chem.* **2016**, *128*, 9443–9446; b) M. Ma, K. Liu, J. Shen, R. Kas, W. A. Smith, *ACS Energy Lett.* **2018**, *3*, 1301–1306; c) H. Zhang, Y. Ma, F. J. Quan, J. J. Huang, F. L. Jia, L. Z. Zhang, *Electrochem. Commun.* **2014**, *46*, 63–66.

[19] Y. Zhai, L. Chiachiarelli, N. Sridhar, *ECS Trans.* **2009**, *19*, 1–13.

[20] a) Q. Lu, J. Rosen, F. Jiao, *ChemCatChem* **2015**, *7*, 38–47; b) J. F. He, A. X. Huang, N. J. J. Jobnson, K. E. Dettelbach, D. M. Weekes, Y. Cao, C. P. Berlinguette, *Inorg. Chem.* **2018**, *57*, 14624–14631.

[21] R. Hinogami, S. Yotsuhashi, M. Deguchi, Y. Zenitani, H. Hashiba, Y. Yamada, *ECS Electrochem. Lett.* **2012**, *1*, H17–H19.

[22] R. Senthil Kumar, S. S. Kumar, M. A. Kulandainathan, *Electrochem. Commun.* **2012**, *25*, 70–73.

[23] Y. L. Wang, P. F. Hou, Z. Wang, P. Kang, *ChemPhysChem* **2017**, *18*, 3142–3147.

[24] X. L. Jiang, H. B. Li, J. P. Xiao, D. F. Gao, R. Si, F. Yang, Y. S. Li, G. X. Wang, X. H. Bao, *Nano Energy* **2018**, *52*, 345–350.

[25] J. Albo, D. Vallejo, G. Beobide, O. Castillo, P. Castano, A. Irabien, *ChemSusChem* **2017**, *10*, 1100–1109.

[26] S. Dou, J. J. Song, S. B. Xi, Y. H. Du, J. Wang, Z. F. Huang, Z. C. J. Xu, X. Wang, *Angew. Chem. Int. Ed.* **2019**, *58*, 4041–4045; *Angew. Chem.* **2019**, *131*, 4081–4085.

[27] L. Ye, J. Liu, Y. Gao, C. Gong, M. Addicoat, T. Heine, C. Wöll, L. Sun, *J. Mater. Chem. A* **2016**, *4*, 15320–15326.

[28] X. Kang, Q. Zhu, X. Sun, J. Hu, J. Zhang, Z. Liu, B. Han, *Chem. Sci.* **2016**, *7*, 266–273.

[29] I. Hod, M. D. Sampson, P. Deria, C. P. Kubiak, O. K. Farha, J. T. Hupp, *ACS Catal.* **2015**, *5*, 6302–6309.

[30] B.-X. Dong, S.-L. Qian, F.-Y. Bu, Y.-C. Wu, L.-G. Feng, Y.-L. Teng, W.-L. Liu, Z.-W. Li, *ACS Appl. Energy Mater.* **2018**, *1*, 4662–4669.

[31] J. X. Wu, S. Z. Hou, X. D. Zhang, M. Xu, H. F. Yang, P. S. Cao, Z. Y. Gu, *Chem. Sci.* **2019**, *10*, 2199–2205.

[32] N. Kornienko, Y. Zhao, C. S. Kley, C. Zhu, D. Kim, S. Lin, C. J. Chang, O. M. Yaghi, P. Yang, *J. Am. Chem. Soc.* **2015**, *137*, 14129–14135.

[33] X. L. Jiang, H. H. Wu, S. J. Chang, R. Si, S. Miao, W. X. Huang, Y. H. Li, G. X. Wang, X. H. Bao, *J. Mater. Chem. A* **2017**, *5*, 19371–19377.

[34] C. W. Kung, C. O. Audu, A. W. Peters, H. Noh, O. K. Farha, J. T. Hupp, *ACS Energy Lett.* **2017**, *2*, 2394–2401.

[35] X. Y. Tan, C. Yu, C. T. Zhao, H. W. Huang, X. C. Yao, X. T. Han, W. Guo, S. Cui, H. L. Huang, J. S. Qiu, *ACS Appl. Mater. Interfaces* **2019**, *11*, 9904–9910.

[36] K. Zhao, Y. M. Liu, X. Quan, S. Chen, H. T. Yu, *ACS Appl. Mater. Interfaces* **2017**, *9*, 5302–5311.

[37] M. K. Kim, H. J. Kim, H. Lim, Y. Kwon, H. M. Jeong, *Electrochim. Acta* **2019**, *306*, 28–34.

[38] Y. F. Ye, F. Cai, H. B. Li, H. H. Wu, G. X. Wang, Y. S. Li, S. Miao, S. H. Xie, R. Si, J. Wang, X. H. Bao, *Nano Energy* **2017**, *38*, 281–289.

[39] C. M. Zhao, X. Y. Dai, T. Yao, W. X. Chen, X. Q. Wang, J. Wang, J. Yang, S. Q. Wei, Y. E. Wu, Y. D. Li, *J. Am. Chem. Soc.* **2017**, *139*, 8078–8081.

[40] F. P. Pan, H. G. Zhang, K. X. Liu, D. Cullen, K. More, M. Y. Wang, Z. X. Feng, G. F. Wang, G. Wu, Y. Li, *ACS Catal.* **2018**, *8*, 3116–3122.

[41] D. H. Nam, O. S. Bushuyev, J. Li, P. De Luna, A. Seifitokaldani, C. T. Dinh, F. P. G. de Arquer, Y. H. Wang, Z. Q. Liang, A. H. Proppe, C. S. Tan, P. Todorovic, O. Shekhah, C. M. Gabardo, J. W. Jo, J. M. Choi, M. J. Choi, S. W. Baek, J. Kim, D. Sinton, S. O. Kelley, M. Eddaoudi, E. H. Sargent, *J. Am. Chem. Soc.* **2018**, *140*, 11378–11386.

[42] X. Q. Wang, Z. Chen, X. Y. Zhao, T. Yao, W. X. Chen, R. You, C. M. Zhao, G. Wu, J. Wang, W. X. Huang, J. L. Yang, X. Hong, S. Q. Wei, Y. Wu, Y. D. Li, *Angew. Chem. Int. Ed.* **2018**, *57*, 1944–1948; *Angew. Chem.* **2018**, *130*, 1962–1966.

[43] W. W. Guo, X. F. Sun, C. J. Chen, D. X. Yang, L. Lu, Y. D. Yang, B. X. Han, *Green Chem.* **2019**, *21*, 503–508.

[44] R. Wang, X. Sun, S. Ould-Chikh, D. Osadchii, F. Bai, F. Kapteijn, J. Gascon, *ACS Appl. Mater. Interfaces* **2018**, *10*, 14751–14758.

[45] Y. Zheng, P. Cheng, J. Xu, J. Han, D. Wang, C. Hao, H. R. Alanagh, C. Long, X. Shi, Z. Tang, *Nanoscale* **2019**, *11*, 4911–4917.

[46] Y. Guo, H. J. Yang, X. Zhou, K. L. Liu, C. Zhang, Z. Y. Zhou, C. Wang, W. B. Lin, *J. Mater. Chem. A* **2017**, *5*, 24867–24873.

[47] a) Z. Weng, J. Jiang, Y. Wu, Z. Wu, X. Guo, K. L. Materna, W. Liu, V. S. Batista, G. W. Brudvig, H. Wang, *J. Am. Chem. Soc.* **2016**, *138*, 8076–8079; b) G. Zhu, Y. Li, H. Zhu, H. Su, S. H. Chan, Q. Sun, *ACS Catal.* **2016**, *6*, 6294–6301; c) S. Lin, C. S. Diercks, Y.-B. Zhang, N. Kornienko, E. M. Nichols, Y. Zhao, A. R. Paris, D. Kim, P. Yang, O. M. Yaghi, C. J. Chang, *Science* **2015**, *349*, 1208–1213.

[48] X. M. Hu, M. H. Ronne, S. U. Pedersen, T. Skrydstrup, K. Daasbjerg, *Angew. Chem. Int. Ed.* **2017**, *56*, 6468–6472; *Angew. Chem.* **2017**, *129*, 6568–6572.

[49] W. W. Kramer, C. C. L. McCrory, *Chem. Sci.* **2016**, *7*, 2506–2515.

[50] F. Schüth, M. D. Ward, J. M. Buriak, *Chem. Mater.* **2018**, *30*, 3599–3600.

[51] *CRC Handbook of Chemistry and Physics, Vol. 85* (Ed.: D. R. Lide), CRC Press, Boca Raton, FL, **2004**.

[52] B. Liu, H. Shioyama, T. Akita, Q. Xu, *J. Am. Chem. Soc.* **2008**, *130*, 5390–5391.

[53] a) R. Walczak, B. Kurpil, A. Savateev, T. Heil, J. Schmidt, Q. Qin, M. Antonietti, M. Oschatz, *Angew. Chem. Int. Ed.* **2018**, *57*, 10765–10770; *Angew. Chem.* **2018**, *130*, 10926–10931; b) M. Antonietti, M. Oschatz, *Adv. Mater.* **2018**, *30*, 1706836.

[54] A. Ramirez, L. Gevers, A. Bavykina, S. Ould-Chikh, J. Gascon, *ACS Catal.* **2018**, *8*, 9174–9182.

[55] T. Burdyny, W. A. Smith, *Energy Environ. Sci.* **2019**, https://doi.org/10.1039/c8ee03134g.